Journal of Materials and Electronic Devices 2 (2025) 83-89

JOURNAL OF MATERIALS AND ELECTRONIC DEVICES
JMED

Degradation of superconducting properties of the boron-doped $FeSe_{0.5}Te_{0.5}$ superconductor system

Mehmet Eyyüphan YAKINCI[1] and Kübra YAKINCI[2]

[1]Iskenderun Technical University, Faculty of Engineering and Natural Sciences, Department of Metallurgy and Materials Engineering, 31200-Iskenderun, Hatay-Türkiye
[2]Iskenderun Technical University, Faculty of Engineering and Natural Sciences, Department of Engineering Fundamentals, 31200-Iskenderun, Hatay-Türkiye

In this study, superconducting samples were prepared using the solid-state method by adding 0, 1, 2, 3, 4, and 5 % boron to the $FeSe_{0.5}Te_{0.5}$ superconductor system. The structural, microstructural, electrical, and magnetic properties of the samples are examined, and the results are presented. The findings show that boron doping disrupted both the structural and electrical conduction mechanisms in the material, leading to the loss of superconductivity as the doping level increased. Structural shrinkage and increased dislocations were observed in the crystal structure. As the doping ratio increased, the normal-state resistivity, the critical transition temperature, and the zero resistance temperature all decreased significantly. The T_c^{on} values decreased from 15.7 K in the undoped sample to 13.9 K in the 5 % boron doped sample, and T_{zero} decreased from 14.8 K in the undoped sample to 10.8 K in the 5 % boron doped sample. Additionally, it was found that the diamagnetic properties deteriorated with increased boron doping and shifted toward ferromagnetic properties, negatively affecting the critical current density.

Keywords: *FeSeTe superconductors, boron doping, magnetic properties*

Submission Date: 01 October 2025
Acceptance Date: 07 December 2025

**Corresponding author: meyyuphan.yakinci@iste.edu.tr*

1. Introduction

The fact that Fe-based superconductors, such as High-Temperature Superconductors (HTS), exhibit a layered structure [1-3] and that magnetism and superconductivity can coexist interestingly [4-7] has brought Fe-based superconductors to the forefront in recent studies. Their anisotropic properties, like those of HTS materials, and their high current density (J_c) values are a significant advantage, particularly for technological applications. In addition, anisotropic properties can provide important information about the fundamental electronic structure of the material, especially regarding the Fermi surface behavior and the effects of atomic vacancies that may occur in the structure, provides important guidance for theoretical studies [8-11].

Therefore, studying Fe-based superconductors is also crucial for understanding the mechanism of superconductivity. In these materials, the ability to achieve high values of the upper critical field (H_{c2}), the critical current density (J_c) being at suitable levels for technological applications, and even the potential to significantly enhance these values through doping or substitution keep Fe-based superconductors at the forefront of scientific research.

In particular, by doping Te instead of Se in β-FeSe superconductors, the critical temperature T_c could be increased up to 15 K, and the B_{c2} value could be raised above 45 T [12]. This has made FeSeTe material more practically usable compared to toxic Fe-based superconductor materials containing As. The relatively high T_c values of FeSeTe materials have been further targeted for increase through

various doping or substitutions. For example, doping with Ag, Cl, Al, Ti, Co, O, Mn, Mg, and F or multi-wall carbon nanotubes (MWCNTs) has produced notable results, both positive and negative [13-16]. Among these, heat treatments with O_2 helped remove excess Fe from the matrix, resulting in significant improvements in transport properties, particularly in current density values [17]. Similarly, the literature reports that F doping positively impacts transport properties [12].

In another study, it was found that Ag doping in both single-crystal and polycrystalline samples reduces Fe impurities, especially at grain boundaries, and promotes the formation of a more transparent grain boundary, leading to significant improvements in electrical transport properties [18]. It was also known that there is a specific chemical solubility limit in the structure due to MWCNT doping, depending on the doping concentration, and that doping within these limits significantly increases the T_c, J_c, and B_{c2} values. In fact, many of these dopings appear to increase the current density of the samples by creating defects or pinning centers. One of the best examples is the strengthening of the pinning mechanism in the matrix through Cl doping into the structure [19].

This study investigates the structural, electrical transport, and magnetic properties of samples produced by adding 1 % - 5 %wt. boron to the $FeSe_{0.5}Te_{0.5}$ superconductor system using the solid-state method, and the results are presented.

2. Experimental

The solid-state method was used for preparing the samples. First, high-purity iron (99.999% Alfa Aesar), selenium (99.999% Alfa Aesar), tellurium (99.999% Alfa Aesar), and boron (98.9% PavTech) powders were weighed in a glove box to achieve the nominal compositions of $FeSe_{0.5}Te_{0.5}B_x$ (x=0, 1, 2, 3, 4, and 5%), then mixed under an argon atmosphere and placed in quartz tubes. The quartz tubes were sealed under vacuum. Initial heat treatments were performed at 650 and 775 °C with constant heating and cooling rates of 1 °C/min (first heat treatments). After each heat treatment, the quartz glass was crushed inside the glove box, and the powders were ground in an agate mortar under an argon atmosphere. The resulting powder mixtures were returned to quartz tubes under vacuum, sealed, and heated to 850 °C with ramps of 1 °C/min. After 26 hours, the temperature was lowered to 425 °C, completing the heat treatment cycle over 120 hours (second heat treatments).

For the structural analysis of the obtained polycrystalline samples, an X-ray powder diffractometer (XRD) was used. The samples were analyzed with the Malvern-Panalytical Empyrean system and the PIXcel 3D detector, using $Cu_{K\alpha}$ radiation between $2\theta = 5°$ and 80°, and structural parameters were calculated through least-squares fitting of the X-ray lines. The data were then verified using the Rietveld refinement program and the ICDD-PDF4 database. For microstructural analysis, a scanning electron microscope (SEM), specifically a Thermo Scientific-FEI Apreo S model equipped with an energy dispersive X-ray spectrometer (EDS), was employed. Electrical transport properties were measured using the Physical Properties Measurement System (Quantum Design; PPMS-9T) under a magnetic field up to 8 T, along with the vibrating sample magnetometer attachment of the PPMS for magnetic properties, conducted at fields up to ± 8 T and temperatures between 5 and 300 K.

3. Results and Discussions

The polycrystalline samples were ground in a glove box under an argon atmosphere until they reached approximately 10 µm in size. Then, XRD analyses were performed at room temperature. The XRD patterns of the samples are shown in Figs. 1 and 2. Example XRD patterns of samples with x=0 and x=5% Boron doping after the first heat treatment are shown in Fig. 1a and b. Other doping ratios also display similar features. After the first heat treatment, it was observed that the

Table 1. Calculated unit cell parameters of the samples.

Sample Doping ratio	$FeSe_{0.5}Te_{0.5}B_x$			
	***a* = *b* (Å)**	***c* (Å)**	**Unit cell volume (Å^3)**	**Crystal structure / S. group**
x = 0%	3.8101	6.2392	90.57	Tetragonal / P4/nmm
x = 1%	3.8088	6.2305	90.39	Tetragonal / P4/nmm
x = 2%	3.8064	6.2237	90.17	Tetragonal / P4/nmm
x = 3%	3.8035	6.2101	89.84	Tetragonal / P4/nmm
x = 4%	3.7970	6.1967	89.34	Tetragonal / P4/nmm
x = 5%	3.7899	6.1879	88.89	Tetragonal / P4/nmm

crystalline phases were not fully developed, and a multiphase structure was present. However, after the second heat treatment cycle, the XRD peaks and impurity phases became clearly visible. All samples showed sharp peaks along the *c*-axis of crystal growth. Furthermore, the crystal structures of all doped and undoped samples were found to be tetragonal and belong to the P4/nmm space group. It was observed that boron doping did not change the tetragonal structure of the samples. However, a slight shift toward higher angles appeared in the peaks as the boron doping level increased. This is likely due to a slight contraction of the structure caused by differences in ionic sizes from boron doping.

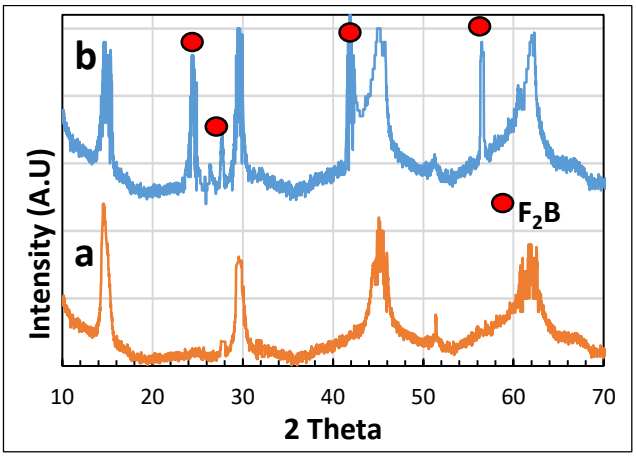

Fig.1. XRD graphs of the samples after the first heating **a)** x=0, and **b)** 0.5% boron-doped samples. The red dot shows the F_2B impurity phase.

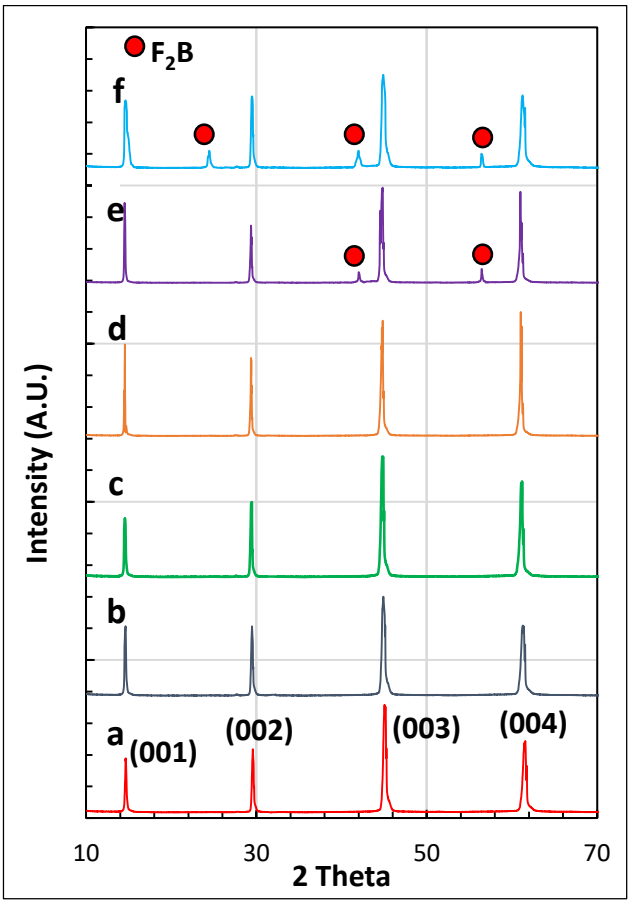

Fig.2. XRD graphs of the samples prepared at the second heating stage **a)** x=0, **b)** 0.1%, **c)** 0.2%, **d)** 0.3%, **e)** 0.4%, and **f)** 0.5% Boron doped samples.

The crystal parameters of the prepared samples are listed in Table 1. As shown in Table 1, as the doping level increases, there is a decrease along the *c*-axis and an elongation along the *a*-axis. It was revealed that the samples shrank as the boron content increased. Furthermore, as the Boron doping rate increases, Fe_2B impurity peaks also appear in the structure, particularly at 4% and 5% boron doping rates.

The results of SEM analyses of the prepared polycrystalline samples are shown in Figs. 3a and b, respectively, for the undoped and the x=5% boron-doped samples as an example. Similar surface morphologies are observed in the other doping rates. However, the only difference was obtained on the grain size of the samples. While the grain structure was smaller in the undoped samples, Fig. 3a, a significant increase was obtained as the doping ratio was increased to 5%, Fig.3b.

Furthermore, it was observed that the structure shrank with the doping, resulting in the formation of cracks or superficial irregularities in the samples. This was more pronounced at the 5% doping ratio. In addition, as seen in Fig. 3b, Fe_2B impurity phase appeared particularly in the highly boron doped samples (circled in white). This became particularly evident, especially starting with the 4% doped samples.

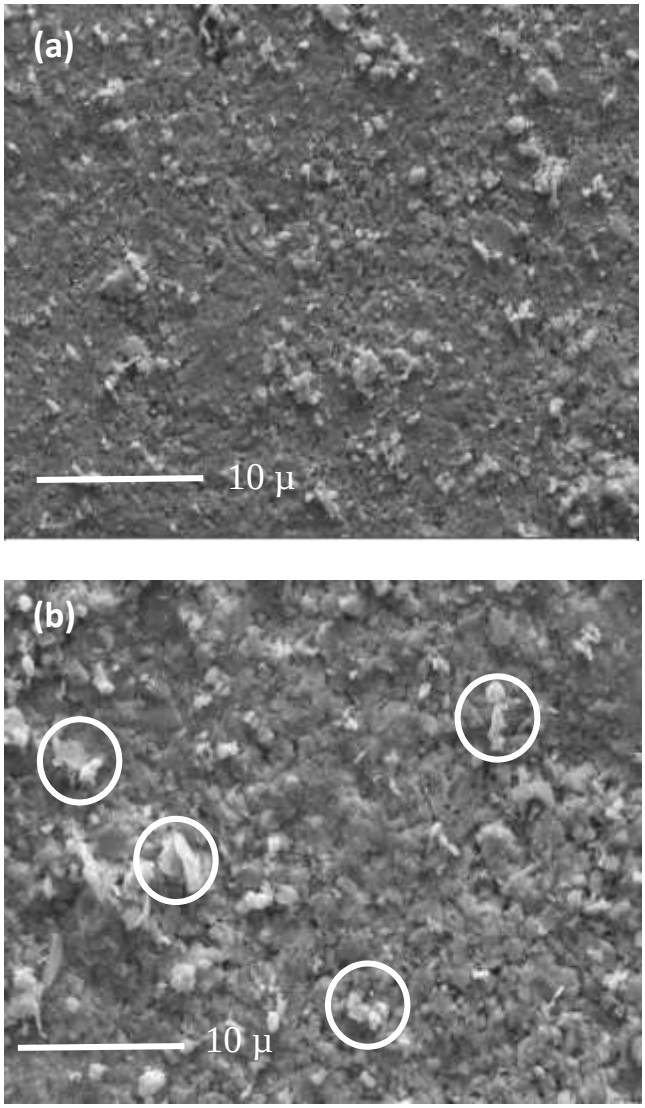

Fig.3. SEM micrographs of **a)** x=0, and **b)** 0.5% boron doped samples. White circles indicate Fe_2B impurity phase.

Table 2. Electrical transport properties of the samples prepared.

Sample		T_c^{on} (K)	T_{zero} (K)	ΔT (K)	J_c^{mag} A/cm^2
$FeTe_{0.5}Se_{0.5}B_x$	0%	15.9	14.9	1	1.4 x 10^5
	1%	15,7	14.4	1.3	6.3 x 10^4
	2%	15.5	14.1	1.4	2.9 x 10^3
	3%	15	13.5	1.5	1.1 x 10^2
	4%	14.3	12.2	2.1	54
	5%	13.9	10.3	3.6	17

The electrical transport properties analysis results of the prepared polycrystalline samples at zero field are presented in Fig. 4. As the doping ratio increased, the normal-state resistivity value, the critical transition temperature (T_c^{on}), and the temperature at which superconductivity begins, T_{zero}, began to decrease significantly. T_{zero} decreased from 14.8 K in the undoped sample to 10.8 K in the 5% doped sample. Similarly, the T_c^{on} values decreased from 15.7 K in the undoped sample to 13.9 K in the 5% doped sample. Consequently, the ΔT (=T_c^{on} - T_{zero}) values of the samples increased systematically with the doping ratio, Fig. 5. According to these results, boron doping in polycrystalline samples negatively affects their superconducting performance.

Figs. 6a and b show the resistivity values of the samples for x=0 and x=5% boron doping under the magnetic fields up to 8 T. The behavior of the other intermediate doping rates exhibits a similar trend. Superconductivity was present in the undoped sample even under an 8 T applied field, Fig.6a, while superconductivity was lost in the 5% boron doped sample starting from an applied 3 T field, Fig.6b. This demonstrates that boron is an incompatible doping agent not only for structural properties but also for electrical transport in the FeSeTe system.

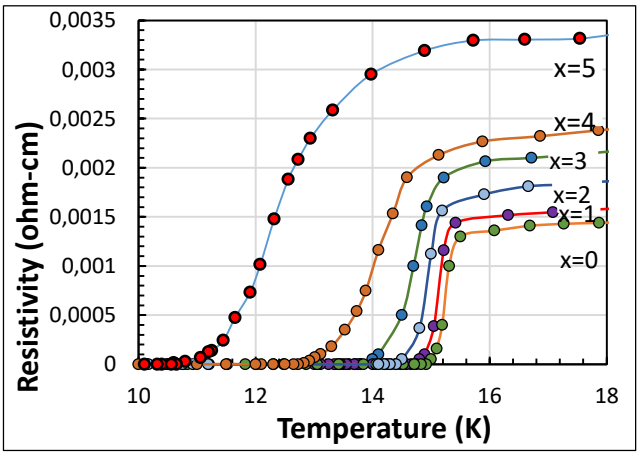

Fig. 4. Resistance versus temperature measurements of the prepared polycrystalline samples.

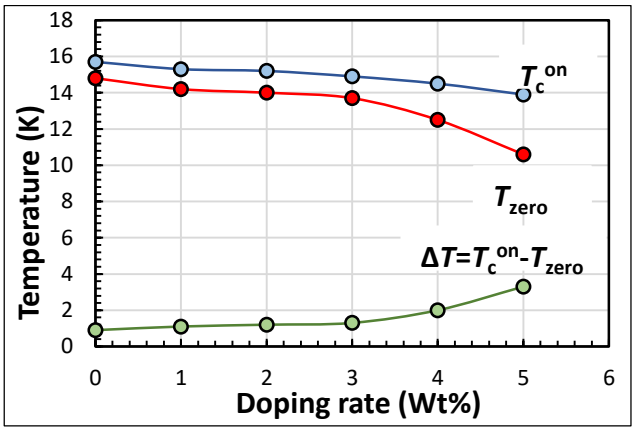

Fig.5. The T_c^{on}, T_{zero} and ΔT values of the samples via doping rate and temperature

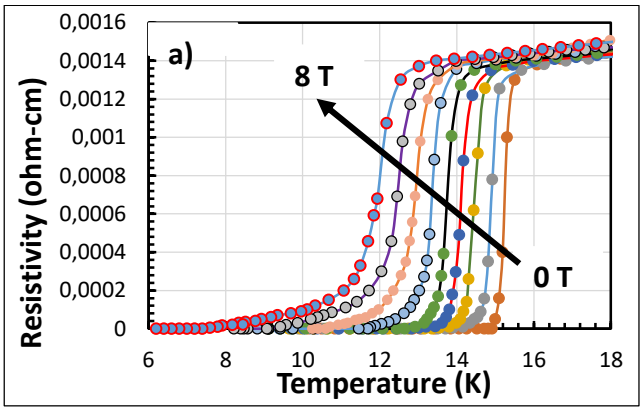

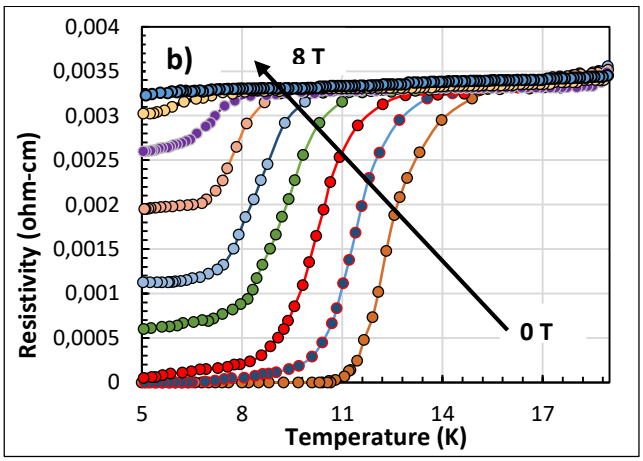

Fig.6. Resistance versus temperature measurements of **a)** x=0% and **b)** x=0.5% boron added sample between 0 - 8 T applied field

This is because, as the boron concentration increases, there is a volumetric shrinkage in the samples due to both the Fe vacancies in the crystal structure and also boron's ionic radius (this is clearly evident in XRD analyses), indicating an increase for dislocations at mainly in 4% and 5% boron added samples.

This obviously suggests that scattering increases due to the increased irregularities in the structure and negatively affects electronic coordination for electrical conduction, ultimately leading to the loss of superconducting performance of the polycrystalline samples prepared in this research.

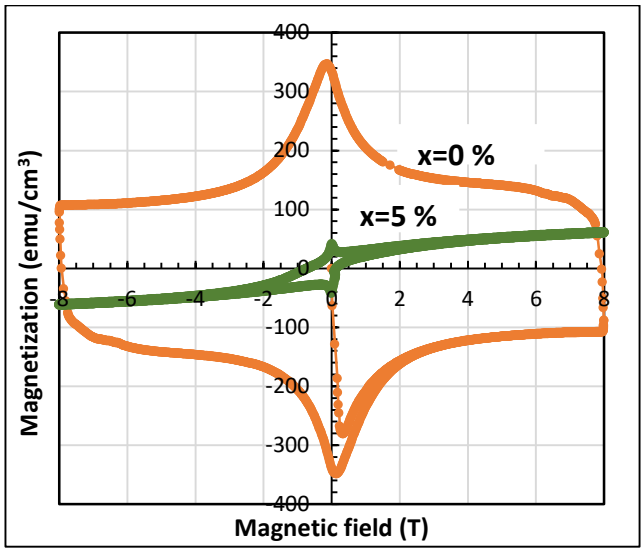

Fig.7. Magnetization versus applied field (*M-H*) measurements of the x=0% and x=5% boron doped samples.

The changes in magnetization of samples doped with boron at x = 0%, 1%, 2%, 3%, 4%, and 5% were investigated at 5 K and under a ±8 T applied magnetic field. Fig. 7 shows the *M-H* plots of samples doped with x = 0% and x = 5% boron for comparison. A fairly broad and conventional HTS type hysteresis curve was obtained in the undoped sample, but it was found that the hysteresis loop wideness decreased significantly as the doping ratio was increased.

The undoped sample exhibited behavior similar to the hysteresis loop of typical Type II superconductors, while the sample doped with boron at x = 5% (the sample exhibiting the weakest superconductivity in this study) exhibited a significantly deteriorated hysteresis curve with increasing field, and the ferromagnetic properties became much more dominant, as shown in Fig. 7.

This ferromagnetic behavior is believed to be due to the shrinkage of the crystal structure and the disruption of the diamagnetic structure by boron atoms settling into the resulting pinning points. This also reveals that the boron atoms are not fully chemically resolved within the matrix, remained unsolved or as Fe_2B phases, and in the form of separate islets thus magnetically ferromagnetic Fe in the matrix become dominant in the structure and this situation manifested itself in the sample as ferromagnetic dominance. Appearance of fully unreacted or Fe_2B boron related phases were clearly evidenced in our XRD and SEM analyses in this work.

The critical current density, J_c^{mag}, values of the samples were calculated using the Bean's model. The Bean model is defined as [20],

$$J_c^{mag} = 20\frac{\Delta M}{a\left(1-\frac{a}{3b}\right)} \quad (1)$$

In Equation 1, a and b are defined as the length of the sample cross-section in cm and are designed so that (a < b). ΔM ($=M_+-M_-$) in the equation is known as the difference between the positive and negative values of the magnetization measured with the applied field in emu cm^{-3}.

It was found that as the boron doping in the samples increased, the J_c^{mag} value decreased accordingly, Fig. 8, and Table 2. Low boron added superconducting samples have fairly high J_c^{mag} values and can be possible to use these materials in technological applications. However, it is particularly noteworthy that the 4% and 5% boron doped samples yielded a J_c^{mag} value below 100 A/cm^2 even in 5 K calculations, which is considered to be a value even worse than that of the conventional metallic conductor materials.

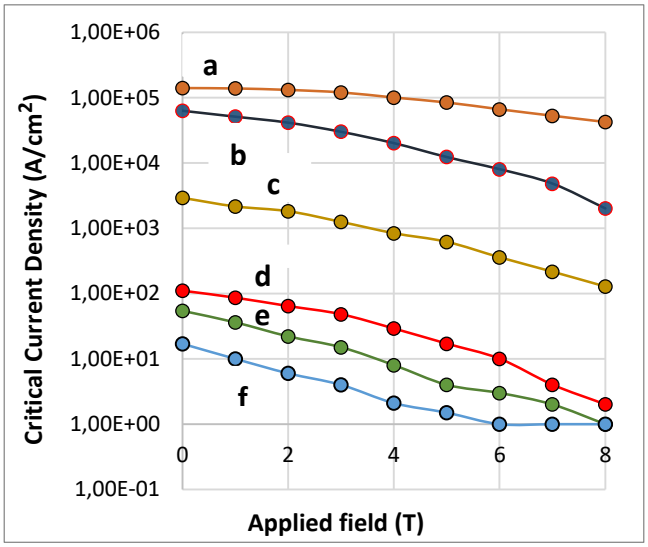

Fig.8. *I-V* calculation results of **a)** x=0, **b)** 0.1%, **c)** 0.2%, **d)** 0.3%, **d)** 0.4% and **f)** 0.5 Boron doped samples.

This demonstrates that boron doping not only degrades the electrical transport properties of the samples but also destroys the effectiveness of the pinning centers in the applied magnetic field which is essential particularly for the high amount of critical current density of the superconductor materials. However, it has been also evaluated that the dislocations formed due to the shrinkage in the structure at high boron doping rates play an important role in obtaining very low current density in our samples prepared in this work.

4. Conclusions

In this study, the FeSeTe superconductor system was doped with 0 to 5% wt. boron and the samples were produced using the solid-state method and double heat treatment procedure. The findings revealed significant structural changes in the produced boron doped material. While the crystal structure and space group remained unchanged, it was found that the *a*- and *c*- parameters of the structure changed with increasing doping, causing volumetric distortion in the matrix. As a result of this distortion, cracks and boron-related impurity phases were observed in the internal structure. This led to the formation of Fe-dominated phases in the structure, leading to significant deterioration in the electrical performance of the samples. While the undoped sample yielded results consistent with the literature, the T_{zero}= 14.9 K value dropped to the T_{zero}= 10.3 K value in the most highly doped sample (x=5%). This situation was even severe under magnetic fields, and superconductivity was found to be lost starting at a 3T applied magnetic field. This situation was also significantly observed in current density values, a key indicator of superconductor quality. While the J_c^{mag} value is around 10^5 A/cm^2 in the undoped sample, this value drops to a very low value of 17 A/cm^2 in the 5% doped sample. This shows that boron doping is not a suitable additive material for FeSeTe alloys and its use, especially in technological applications, will be limited.

References

[1] F.C. Hsu, J. Y. Luo, K.W. Yeh, T. K. Chen, T.W. Huang, P.M. Wu, Y.C. Lee, Y.L. Huang, Y.Y. Chu, D.C. Yan, M.K. Wu: Superconductivity in the PbO-type structure α-FeSe. Proc. Natl. Acad. Sci. U.S.A. (2008). https:// doi. org/ 10. 1073/ pnas. 08073 25105.

[2] X. Liu, L. Zhao, S. He, J. He, D. Liu, D. Mou, B. Shen, Y. Hu, J. Huang, X.J. Zhou: Electronic structure and superconductivity of FeSe-related superconductors. J. Phys. Condens. Matter (2015). https:// doi. org/ 10. 1088/ 0953- 8984/ 27/ 18/ 183201.

[3] K.W. Yeh, T.W. Huang, Y.L. Huang, T.K. Chen, F.C. Hsu, P.M. Wu, Y.C. Lee, Y.Y. Chu, C.L. Chen, J.Y. Luo, D.C. Yan, M.K. Wu: Tellurium substitution effect on superconductivity of the α-phase iron selenide. Europhys. Lett. (2008). https:// doi. org/ 10. 1209/ 0295- 5075/ 84/ 37002.

[4] M. Rotter, M. Tegel, D. Johrendt: Superconductivity at 38 K in the iron arsenide (Ba1−xKxFe2As2. Phys. Rev. Lett. (2008). https:// doi. org/ 10. 1103/ PhysR evLett. 101. 107006.

[5] Y. Ma.: Progress in wire fabrication of iron-based superconductors. Supercond. Sci. Technol. (2012). https:// doi. org/ 10. 1088/0953- 2048/ 25/ 11/ 113001.

[6] H. Hosono, K. Kuroki: Iron-based superconductors: current status of materials and pairing mechanism. Physica C (2015). https:// doi. org/ 10. 1016/j. 2015. 02. 020.

[7] H. Lin, C. Yao, X. Zhang, H. Zhang, Q. Zhang, D. Wang, C. Dong, Y. Ma, Effect of metal (Zn/In/Pb) additions on the microstructures and superconducting properties of Sr1-xKxFe2As2 tapes. Scr. Mater. (2016). https:// doi. org/ 10. 1016/j. scrip tamat. 2015. 09. 031.

[8] **C.** Gong, Q. Zhao, X. Ping, P. Zhang, Y. Liu, L. Hao: Effect of minor graphene doping on the microstructure and superconductivity of FeSe. J. Mater. Sci. Mater. Electron. (2020). https:// doi. org/ 10. 1007/ s10854- 020- 04097-w.

[9] N. Chen, Z. Ma, Y. Liu, X. Li, Q. Cai, H. Li, L. Yu: Infuence of Sn doping on the phase formation and superconductivity of FeSe0.93. J. Alloys Compd. (2014). https:// doi. org/ 10. 1016/j. jallc om.2013. 11. 121.

[10] K. Fabitha, M.S. Ramachandra Rao, M. Muralidhar, K. Furutani, M. Murakami: Effect of Ag addition on microstructure and Raman vibrational modes of bulk FeSe. J. Supercond. Nov. Magn. (2017). https:// doi. org/ 10. 1007/ s10948- 017- 4117-2.

[11] W.B. Qiu, Z.Q. Ma, Y.C. Liu, M.S.A. Hossain, X.L. Wang, C.B. Cai, S.X. Dou: Tuning superconductivity in FeSe thin films via magnesium doping. ACS Appl. Mater. Interfaces (2016). https:// doi. org/ 10. 1021/ acsami. 6b005 74.

[12] K. Deguchi, Y. Takano, Y. Mizuguchi: Physics and chemistry of layered chalcogenide superconductors. Sci. Technol. Adv. Mater. (2012). https:// doi. org/ 10. 1088/ 1468- 6996/ 13/5/ 054303.

[13] Y. Mizuguchi, F. Tomioka, S. Yamaguchi, Y. Takano: Substitution effects on FeSe superconductor. J. Phys. Soc. Jpn. (2009). https:// doi. org/ 10. 1143/ JPSJ. 78. 074712

[14] X.B. Zhu, W.H. Song, Z.R. Yang: Divergency of SDW and structure transition in Fe1−xNixSe0.82 superconductors. Phys. C (2009). https:// doi. org/ 10. 1016/j. physc. 2009. 07. 003

[15] M. Ozabaci, K. Yakinci, M.E. Yakinci: Enhancement of magnetic and transport properties of superconducting $Fe_{1-x}Mn_xSe_{0.5}Te_{0.5}$ crystals. JOM (2019). https:// doi. org/ 10. 1007/ s11837- 019- 03651-0.

[16] N. Chen, Y. Liu, Z. Ma, H. Li: Significant enhancement of superconducting properties in the FeSe0.5Te0.5 bulks by minör Sn addition. Mater. Lett. (2016). https:// doi. org/ 10. 1016/j. matlet.2016. 03. 137

[17] M. K. Wu, M. J. Wang, K. W. Yeh. Recent advances in β-$FeSe_{1-x}$ and related superconductors. Science and Technology of Advanced Materials. (2013). https://doi.org/10.1088/1468-6996/14/1/014402.

[18] K. Yakinci. Study on the Field-Dependent Activation Energy, $U(H,T)$, Upper Critical Field, $H_{c2}(0)$, and Irreversibility Field, $\mu_0 H_{irr}$, Properties of Superconducting Single-Crystal Ag-Added Fe(Se,Te) Alloys. J Supercond Nov Magn**.** (2022). https://doi.or/10.1007/s10948-022-06328-z.

[19] J. Zhao, J. Liao, C. Dong, D. Wang, Y. Ma. Properties and Applications of Iron Chalcogenide Superconductors. *Materials*. (2024).https://doi.org/10.3390/ma17133059

[20] C. Y. Liu, H. Zhang, K. Zhao, F. G. Cai, X. S. Yang, and Y. Zhao, Increased critical current density in iron selenide telluride crystals doping with trace amount of cobalt. J. Appl. Phys. (2025). doi: 10.1063/5.0252231.